Tuning Photocatalytic Activity and Decomposition Properties of Poly(Polyethylene Glycol Diacrylate-co-Hydroxyethyl Methacrylate)/TiO_2 Composite Hydrogel

[1]Melek Tezcan, [1]Huseyin Cicek*, [2]Meryem Cicek and [3]Said Nadeem
[1]*Mugla Sitki Kocman University, Faculty of Science, Department of Chemistry, Kotekli, 48000, Mugla, Turkey.*
[2]*Mugla Sitki Kocman University, Environmental Problems Research and Application Center, Kotekli, 48000, Mugla, Turkey.*
[3]*Aydın Adnan Menderes University, Kosk Vocational School, Department of Food Processing, Kosk-09100 Aydin, Turkey.*
hcicek@mu.edu.tr*

(Received on 16th April 2018, accepted in revised form 17th April 2019)

Summary: We have synthesized TiO_2-loaded porous polyethylene glycol diacrylate-co-hydroxyethyl methacrylate (poly(PEGDA-co-HEMA)) hydrogel composites having tunable photocatalytic properties with structural decomposition. TiO_2 was loaded over hydrogels by impregnation of titanium oxobutyrate ($Ti(OBu)_4$), peptized at room temperature that resulted poly(PEGDA-co-HEMA)/TiO_2 composites. Pore morphology, crystalline structure and TiO_2 content of the hydrogels/composites were examined using SEM, XRD and TGA analyses. Structural decomposition rate of the composite hydrogels and model contaminant (methyl orange) was performed under simulated sun light. Suitable pore size, morphology and higher PEGDA/HEMA ratio in the formulation increased the structural decomposition rate of the polymer that works as a TiO_2 template. As the template breaks out, it leaves behind a porous TiO_2 skeleton – thus accelerates the photocatalytic activity. Although the TiO_2 template did not formed at lower PEGDA/HEMA ratio and lower molecular weight of PEGDA, decomposition rate of the composite slowed down (10 % in 108 h). The prepared hydrogels can be used in the skin care & engineering and waste water treatments.

Keywords: Hydrogel, TiO_2 photocatalyst, Polymer–TiO_2 composite**,** Photocatalytic decomposition.

Introduction

Sea is a natural sink for most of the fresh/waste water. It must accommodate both inorganic and organic contaminants. Several methods have been reported to decompose the organic contaminants *i.e*. antibiotics, dyes and phenolics etc. but they are not environmental friendly [1–3]. There are recent studies on photocatalytic techniques to decompose the organic contaminants in waste water [4–6]. Rutile and anatase crystal forms of TiO_2 are successful decomposers [7]. TiO_2 nanocrystal provides high surface area, thus shows high photocatalytic activity [8].

Polymeric carriers with photocatalytic properties have been achieved by entrapping TiO_2 powders in polymeric films [9–11]. The breaking away of TiO_2 nanoparticles from its carrier during the utilization is the basic problem in this method. These micro- and nanoparticles need to be separated by high speed centrifugation, their use in photocatalytic activities is unpractical. In another method, inorganic precursors are absorbed on the polymeric microparticles by layering and calcination at high temperatures followed by sol-gel formation to obtain TiO_2 crystalline skeleton[12]. However, it may cause deformation to the crystal morphology, thus reduce the photocatalytic activity.

In certain procedures, TiO_2 particles are entrapped in the polymers, but during the decomposition, the polymers degrades or to be degraded. TiO2 nanoparticles were immobilized in temperature-sensitive NIPAM (N-isopropylacrylamide)-based polymeric hydrogels and notable temperature-tunable photocatalytic activities were observed with the loss of weight [13]. However, green chemistry needs self-degradable polymers e.g. acrylate [14,15] and chitosan-based composites [16]. In addition, TiO_2 containing composite polymeric films are commonly preferred in skin tissue engineering to accelerate its decomposition and balance the hydrophilicity [17]. Photocatalytic degradation should occur in a short time. It is beneficial in skin tissue applications, although, it has disadvantages in long term usage e.g. decomposition of organic contaminants from waste water.

***To whom all correspondence should be addressed.**

In a study, fluorine carrying nanofibers impregnated with titanium oxosulphate ($TiOSO_4$) by electrospinning and autoclaved at 150 ^oC were used to obtain TiO_2-fluoro composite nanofibers [18]. These nanofibers can protect their integrity and photocatalytic activity, even when used for 10 times. However, the production of nanofiber forms requires a very long production time and high temperatures. These nanofibers are fragile enough to be used in harsh environmental conditions. Padhi and coworkers have studied the mechanical and morphological properties of halloysite nanotubes filled ethylene-vinyl acetate copolymer nanocomposites and analyzed by FTIR and SEM images[19]. On the other hand, Wang et al studied the synthesis of highly crystalline mesoporous TiO2 by a fast sol-gel method.[20] in another study, Pt nanoparticles were supported on mesoporous ZSM-5 and studies for its potential as catalyst for reforming methane with carbon dioxide.[21]

The above discussion reflects that there was a need macro-sized TiO_2 carriers that should be easily producible, photocatalytically effective, large, structurally stable and can be produce at room temperatures. Acid peptization at medium temperatures followed by inorganic precursor absorption over polymeric carriers is one of the alternative and easier methods to obtain TiO_2 crystals when compared to other methods [22–25]. To the best our knowledge, there is no study that produces photocatalytically active composite hydrogels at room temperature by acid peptization, tune its photocatalytic performance and decomposition properties by changing structure and morphology of composites. Herein we report macro-sized poly(PEGDA-co-HEMA)/TiO_2 composite hydrogels (approx. 1 cm diameter, 2 mm thickness) whose decomposition rate can be tuned by adjusting its formulations. We have selected the poly(PEGDA-co-HEMA) as it is biocompatible, non-cytotoxic and environmental friendly.

Experimental

Materials

Anhydrous benzene (99.5 %, Panreac), dried over metallic sodium, was used as a solvent to synthesize divinyl-terminated PEGDA macrocroslinker of different molecular weights[26,27]. Triethylenamine (TEA) (99 %, Sigma–Aldrich), acrylate chloride (AC) (Aldrich) and PEG of different molecular weights (Mn: 400; 2,000; 4,000; 8,000 and 20,000 g/mol) were used as reactants. Synthesized PEGDA macrocrosslinkers were precipitated using hexane (95 %, Sigma-Aldrich) and diethyl ether (J.T. Baker 99. 5 %). Poly(PEGDA-co-HEMA) hydrogels were prepared using PEGDA at different molecular weights, HEMA [(97 %, Sigma-Aldrich), APS (98 %, Sigma-Aldrich)] and TEMED (99 %, Sigma-Aldrich) as monomer, co-monomer, initiator and accelerator, respectively. Porosity in hydrogels was created with PEG of different molecular weights and sodium bicarbonate ($NaHCO_3$) (Merck). $Ti(OBu)_4$ (97 %, Aldrich) was selected as a precursor molecule to obtain TiO_2/poly(PEGDA-co-HEMA) composite hydrogel matrix [28,29]. Nitric acid (65 %, Merck) was used for peptization of this precursor molecule to crystallize TiO_2 layers. Methyl orange (MO) was used in photocatalytic activities as a model contaminant.

Preparation of Poly(PEGDA-co-HEMA) hydrogel matrices

Poly(PEGDA-co-HEMA) hydrogel matrices were produced using the formulations given in Table-1. PEGDA macromonomer of known molecular weight (Table-1) was dissolved in 2 % acetic acid solution in a plastic tube (internal diameter 9 mm), to which, PEG and/or $NaHCO_3$ was/were dissolved. To initiate hydrogel formation, 0.1 mL APS (10 % aqueous), and 0.1 mL TEMED (10 % aqueous) were agitatedly added to this mixture under nitrogen environment. After 24 hours, hydrogels were removed from the tubes and cut in disc forms (approx. 2 mm thick). All hydrogel discs were cleansed with distilled water several times to develop pores as the PEG and in case of $NaHCO_3$, CO_2 produced removes from the matrix.

TiO_2 Loading on Poly(PEGDA-co-HEMA) hydrogels

We have developed the procedure to load TiO_2 on Poly(PEGDA-co-HEMA) hydrogels but got the basic idea from literature [24]. Wet and swollen water equilibrated hydrogel discs were taken in 2 mL 90:10 $Ti(OBu)_4$:ethanol (v/v) mixture in a Pyrex glass tube. The mixture was sonicated for 10 seconds after each 5 minutes, for total 6 times. $Ti(OBu)_4$ hydrolyzes to give titanate after which, condensation occurs to provide interconnected TiO_2 moieties as well as with the –OH of poly(HEMA) in the hydrogel matrix. Prepared hydrogels were filtered, peptized by 2 mL 0.1 mol L^{-1} HNO_3 and stored in the dark for two days. Again, 2 mL 0.1 mol L^{-1} HNO_3 was dropped over the swollen hydrogel discs and left for 15 minutes to terminate peptization. Hydrogel discs were sonicated in distilled water to remove the TiO_2 layers that were not physiosorbed.

Table-1: Different formulations for production of poly(PEGDA-co-HEMA) hydrogels.

Hydrogel code	Molecular weight of PEGDA (g/mol)	Amount of PEGDA (g)	Amount of water (mL)	Acetic acid[a] (mL)	Molecular weight of PEG (g/mol)	Amount of PEG (g)	Amount of HEMA (mL)	APS[b] (mL)	TEMED[b] (mL)	$NaHCO_3$ (g)
P4	4000	0.16	-	1	20000	0.25	0.08	0.07	0.07	0.006
P5	4000	0.32	-	1	20000	0.25	0.16	0.07	0.07	0.006
P6	4000	0.16	-	1	8000	0.25	0.08	0.07	0.07	0.006
P7	4000	0.12	-	1	20000	0.25	0.06	0.07	0.07	0.006
P9	4000	0,16	-	1	400	0,25	0,08	0,07	0,07	0,006
P16	4000	0.16	1	-	20000	0.25	0.08	0.07	0.07	-
P17	4000	0.16	1	-	8000	0.25	0.08	0.07	0.07	-
P18	4000	0.16	1	-	4000	0.25	0.08	0.07	0.07	-
P20	4000	0.16	1	-	400	0.25	0.08	0.07	0.07	-
P22	4000	0.44	-	1	20000	0.25	0.04	0.07	0.07	0.006
P23	4000	0.40	-	1	20000	0.25	0.08	0.07	0.07	0.006
P24	4000	0.32	-	1	20000	0.25	0.16	0.07	0.07	0.006
P25	4000	0.24	-	1	20000	0.25	0.24	0.07	0.07	0.006
P26	4000	0.16	-	1	20000	0.25	0.32	0.07	0.07	0.006
P27	2000	0.32	-	1	20000	0.25	0.16	0.07	0.07	0.006
P28	8000	0.32	-	1	20000	0.25	0.16	0.07	0.07	0.006
P30	4000	0.32	1		20000	0.25	0.16	0.07	0.07	0.006
P31	4000	0.04	-	1	20000	0.25	0.44	0.07	0.07	0.006
P32	4000	0.08	-	1	20000	0.25	0.40	0.07	0.07	0.006
P35	4000	0.04	-	1	20000	0.25	0.44	0.07	0.07	0.012
P36	4000	0.04	-	1	20000	0.25	0.44	0.07	0.07	0.024
P37	4000	0.04	-	1	20000	0.25	0.44	0.07	0.07	-
P38	4000	0.04	1	-	20000	0.25	0.44	0.07	0.07	-
P39	4000	0.04	1	-	-	-	0.44	0.07	0.07	-
P40	4000	0.04	1	-	20000	0.05	0.44	0.07	0.07	-
P41	2000	0.015	-	1	20000	0.25	0.165	0.07	0.07	0.006
P42	2000	0.015	-	1	-	-	0.165	0.07	0.07	0.006
P44	400	0.015	-	1	-	-	0.165	0.07	0.07	0.006

[a]2% water solution, [b] 10% water solution

Characterization

Samples were dried in a vacuum oven at 40 °C and characterized using FTIR (Thermo Scientific Nicolet iS10). Pore size and morphology were determined by Scanning Electron Microscopy (SEM) (JSM-7600 F FEG). For SEM analyses, samples were freeze dried (Martin Christ Freeze Dryers GmbH, Osterode an Harz) at -80 °C for 48 hours and lyophilized at 0 °C and 0.1 mbar for 24 hours. The prepared samples were coated with a gold layer. Composite hydrogel crystals were analyzed by X-Ray Diffraction (XRD) (Rigaku). The TiO_2 content of the dried hydrogels were determined by thermal gravimetric analysis (TGA) (Perkin Elmer-TGA400) under nitrogen atmosphere (30–700 °C, 10 °C/min gradient). TiO_2 content of hydrogels was calculated according to Equation 1.

$$\mathbf{TiO_2\ loading\ (\%)} = \frac{\mathbf{W_{TGA}}}{\mathbf{Wi}} \mathbf{x\ 100} \qquad (1)$$

where, W_i and W_{TGA} represents dry sample weight of TiO_2 containing hydrogel and its weight remaining after TGA test, respectively. DSC measurement was performed with Perkin Elmer DSC-8000 under nitrogen atmosphere (30–150 °C, 10 °C/min gradient). Photocatalytic activity was performed by a mechanical shaker (100 cpm) under three lamps (Osram Ultra Vitalux 300W) with 45,000 lux light intensity representing real sunlight. Composite hydrogel disc and 30 mL 5 ppm MO solution and were left for 30 minutes in the dark to check the amount of MO adsorbed in the composite, that was almost negligible. The mixture was shaken at 50 cpm under lamps. At various times, samples were subjected to spectrophotometric analyses at 465 nm (Schimatzu UV-visible spectrophotometer). Photocatalytic activity of composite hydrogels as mg MO/hour were calculated using Equation 2.

$$\mathbf{Photocatalytic\ activity} = \left[\frac{\mathbf{Ao - At}}{\boldsymbol{\alpha}}\right] \mathbf{x}\ \frac{\mathbf{V}}{\mathbf{t}} \qquad (2)$$

where A_o, A_t, α, V and t represent MO absorbance before (left for 30 min in the dark) photocatalytic activity, MO absorbance at different time periods, slope (absorbance/ppm) of calibration curve, total volume of solution in beaker (L) and time for photocatalytic experiment (hour), respectively. Thickness and diameter of hydrogels were measured (approx.) with a caliper to calculate external surface area and volume of hydrogel discs.

Structural decomposition of composite hydrogels during photocatalytic activity was examined by gravimetric, FTIR and SEM analyses. The decomposition rate of TiO_2/poly(PEGDA-co-HEMA) composite hydrogels were determined as decomposition percent of composite hydrogel per hour (eq. 3).

$$\textbf{Decomposition rate} = \frac{(Wi - Ws)}{Wi \times td} \times 100$$

= decomposition percent / t_d (3)

where W_i, W_s and t_d represent initial dry weights of hydrogels (g), dry weights of hydrogels at the end of photocatalytic activity (g) and time of experiment (hour), respectively.

Results and discussion

Synthesis of PEGDA

FTIR analyses of synthesized PEGDA and its precursor PEG macromolecules are given in Fig 1. A small shoulder related to C=C band is visible at 1610 cm^{-1} in the spectrum of PEGDA, which is not available in the spectrum of PEG, shows the formation of PEGDA macromolecules. Similar bands have been reported for the reaction of hydroxyl group of PEG and chloride group of acrylate chloride [30]. The band in PEG related to hydroxyl around 3500-3400 cm^{-1} also disappeared that supports the idea of the conversion of -OH to reactive C=C group – a monomer. During the conversion of monomers into polymers, double bonds are being consumed [31,32]. This behavior was observed during the preparation of poly(PEGDA-co-HEMA) hydrogels. The C=C band in HEMA and in PEGDA at 1610 cm^{-1} disappeared in the copolymeric poly(PEGDA-co-HEMA) hydrogels.

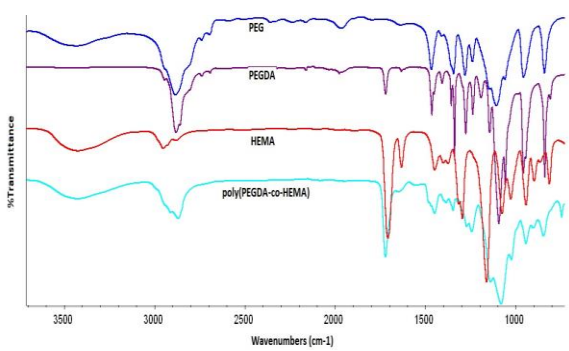

Fig. 1: FTIR spectrums of: A) PEG, B) PEGDA, C) HEMA and D) poly(PEGDA-co-HEMA) hydrogels

Production of TiO_2/poly (PEGDA-co-HEMA) composite hydrogels

TiO_2 loading on poly(PEGDA-co-HEMA) hydrogels takes place in three steps. In the first step, hydrogel absorbs aqueous $Ti(OBu)_4$. In the second step, monomers are being hydrolyzed while in the last step, these molecules' starts to produce TiO_2 layers by condensing both itself and hydroxyls of the copolymer. After that, acid peptization occurs where HNO_3 molecules penetrates hydrogel. Ti-OH bonds dehydrates to form new Ti-O-Ti (titanate) bonds or Ti-O-H-O-Ti hydrogen bonds [24,25]. Two TiO_2/poly(PEGDA-co-HEMA) composites *i.e.* P14 and P14 were analyzed by FTIR spectrums. These composites showed high TiO_2 loading in the case of P4 (35 %) while relatively low in P14 (15 %); obtained from TGA analysis.

XRD analysis

According to the literature, 2θ values for anatase are 25, 38, 48, 54, 55 and 63 while for rutile are 28, 36, 42, 55 and 63 [25,33]. XRD spectra of hydrogels before and after the TiO_2 loading are given in Fig. 2A and B, respectively. 2θ values of 19, 24 and 36 were observed prior to TiO_2 loadings that shows the crystalline regions in the hydrogels (Fig. 2A). After TiO_2 loading, new peaks were appeared in the spectrum at 22, 27, 28, 33, 38, 44, 56, 65 and 78 that show the TiO_2 presence in the hydrogel composite. After the composite formation, the area under peak at 24 increased as compared to the area under the peak at 19, it means that there might a peak at 19. In addition to, the peak at 38 is normally found in anatase type of crystals. Except the 2θ peak at 22, other peaks are near to the rutile form of crystals. We can say that the composite consists of both rutile and anatase crystals as reported earlier [24]. The peaks were also broad that shows the nano-powder formation [33].

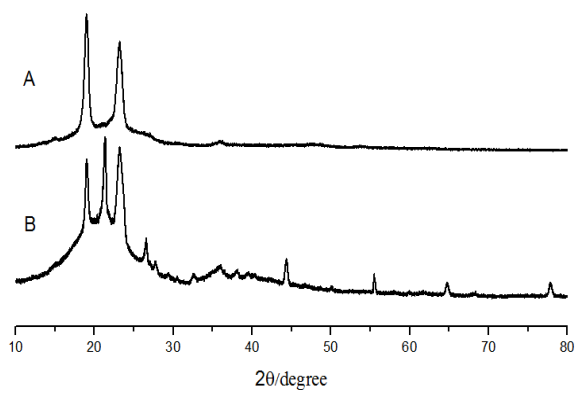

Fig. 2: XRD results: A) P22 without the addition of TiO_2; B) P22 loaded with TiO_2.

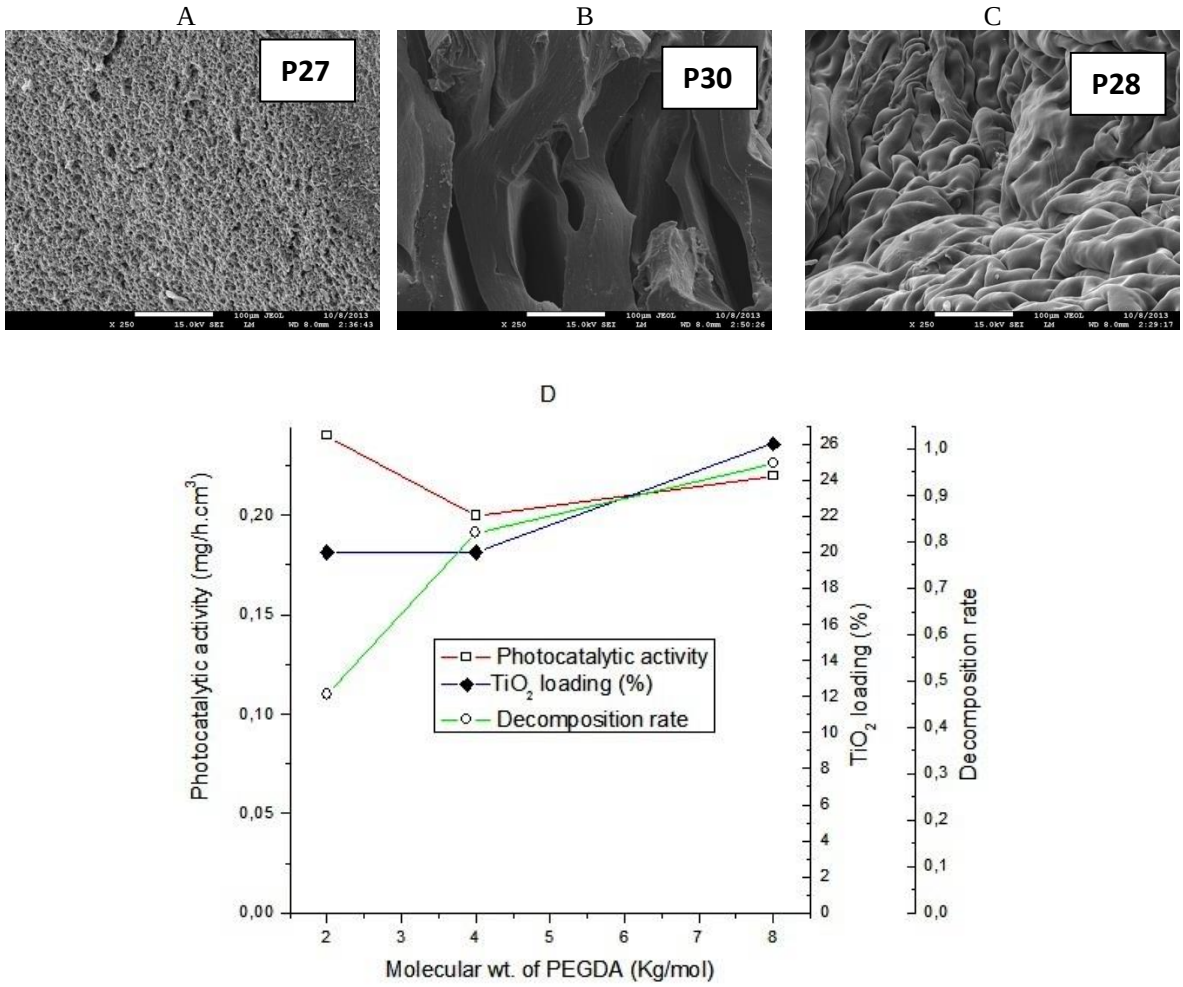

Fig. 3: TEM images showing the effects of PEGDA molecular weight on pore morphology of P27 (A), P30 (B) and P28 (C) coded poly(PEGDA-co-HEMA) hydrogels and on photocatalytic reduction rate, TiO_2 content and decomposition rate (D) of their TiO_2 composites.

Effect of PEGDA molecular weight

SEM photographs (Fig. 3 A, B, C) of poly(PEGDA-co-HEMA) hydrogels synthesized from different molecular weights of PEGDA (2, 4, 8 Kg mol^{-1}) together with the photocatalytic activity, TiO_2 loadings and decomposition rate of their composites are given in Fig. 3D, respectively. Although the similar amounts of TiO_2 was loaded over the hydrogels of various PEGDA molecular weights, higher photocatalytic activity against MO was observed at lower molecular weights of PEGDA, due to the small pore size (*i.e.* higher surface area) of P27 as clearly visible from Fig. 3 A. On the other hand, hydrogels with 4 and 8 Kg mol^{-1} of PEGDA provided wider pores (less surface area), thus it showed less photocatalytic activity. Moreover, high cross-linking density with low PEGDA molecular weight causes less decomposition rate of composite hydrogels. Here, changing the PEGDA molecular weight gives the tuning property to the composite hydrogels. While being used at the commercial level, the user can tune the decomposition rate of the composite per their needs.

Effect of pore formers

In this study, two types of pore formers *i.e.* PEG (0.4, 4, 8, 20 Kg mol^{-1} and different amounts) and $NaHCO_3$ (different amounts) were used. $NaHCO_3$ is macro- while PEG is micropore former. The aim was to prepare pores of both macro and microsize [34]. By this way, we can have a hydrogel where TiO_2 particles of macro size would be interconnected by micro TiO_2 networks. So, when the hydrogel is decomposed, we will have a fine TiO_2 networks connected to coarse TiO_2 particles. To have a more suitable TiO_2 network, PEG molecular weight and amounts of $NaHCO_3$ were tuned.

Out of the tested samples, P20 and P16 are important to discuss. Results of poly(PEGDA-co-HEMA) hydrogels with different molecular weight of PEG are given in Fig. 4A-E. Hydrogel P20 was synthesized using a lower molecular weight of PEG (0.4 Kg mol^{-1}), while the P16 was prepared with higher PEG amounts (20 Kg mol^{-1}). TiO_2 loadings on the composites were almost similar (Fig. 4A). During the photocatalytic activity of the composites against MO, photocatalytic activity and decomposition rate (Fig. 4A) were found as inversely proportional to the molecular weight of PEG in the composites. The reason was observed after the samples were subjected to the SEM analyses. In P20 (Fig. 4D) and its TiO_2 loaded form (Fig. 4E), the pores are available to the incoming adsorbents. On the other hand, P16 (Fig. 4B) and its TiO_2 loaded images (Fig. 4C) showed that the surface area is wavy and no pores are available.

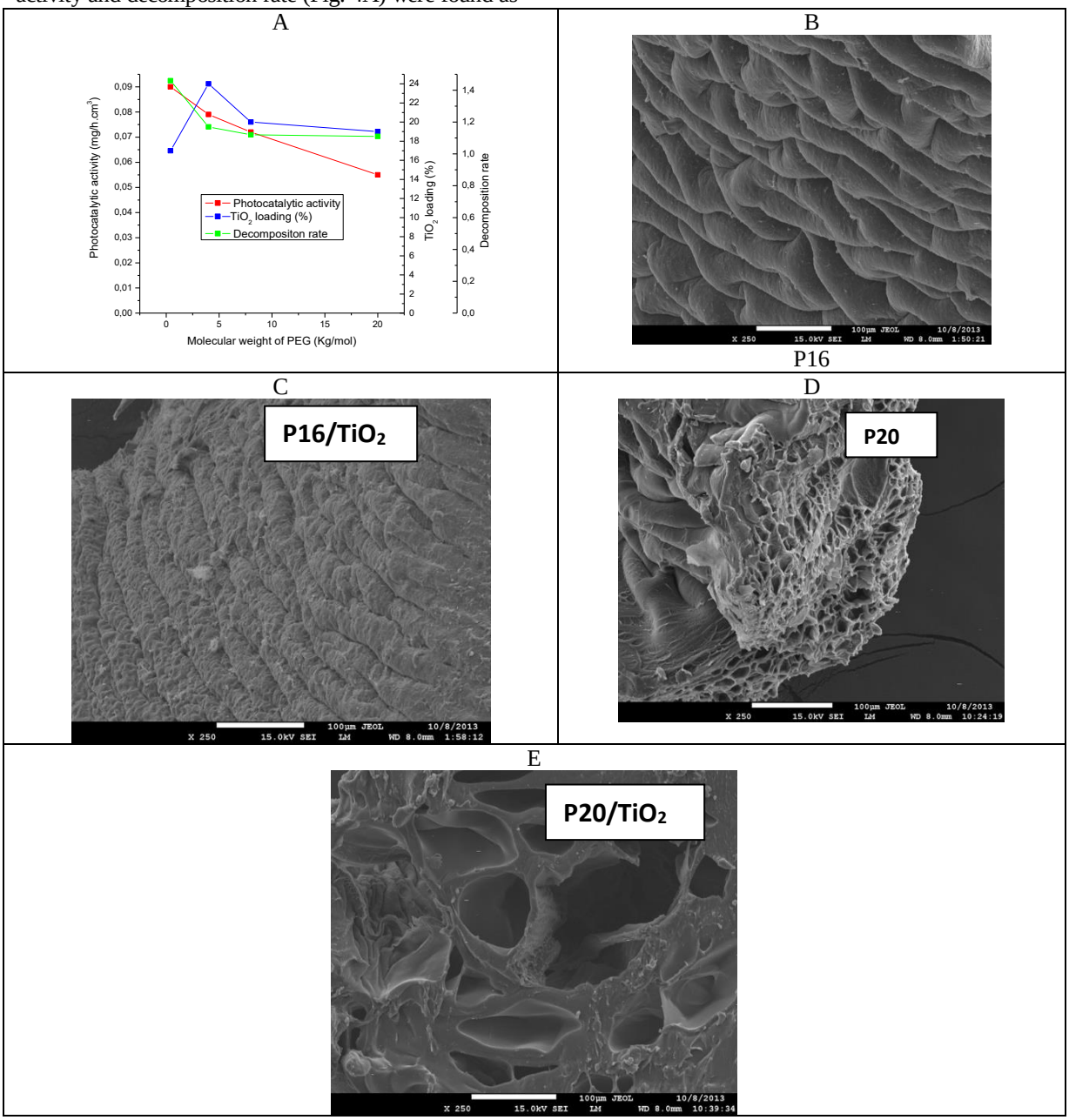

Fig. 4: TEM images showing the effects of PEG molecular weight on photocatalytic reduction rate, TiO_2 content and decomposition rate of their TiO_2 composites and pore morphology of P16, and P20 coded poly(PEGDA-co-HEMA) hydrogels before (A and C) and after (B and D) TiO_2 loading.

The amount of secondary pore former *i.e.* $NaHCO_3$ was changed between 0.0–0.24 g in various formulations. TiO_2 content, photocatalytic rate and decomposition rate of composite hydrogels are provided in Fig. 5. It is well known that high amounts of $NaHCO_3$ causes the formation of wide, heterogeneous and interconnected pores in hydrogels [35]. In our study, this behavior was also observed in the case of TiO_2 loadings. At higher amounts of $NaHCO_3$ *i.e.* 0.024 g, the amount of loaded TiO_2 almost doubled. At less amounts *i.e.* 0.006 g, less TiO_2 was loaded but the pores were of suitable morphology that was also observed from the photocatalytic activity. As the amount of $NaHCO_3$ was increased, the photocatalytic of the composites against the MO was decreased. In addition, the decomposition of the MO occurs mainly on composite surface while the composite decomposes wherever sunlight reaches. That is why the rise in the decomposition of composite was expected with increasing the surface area with due to more $NaHCO_3$. More CO_2 will evolve to left behind larger pores to expose them to sunlight. In that case, sunlight also goes inside the pores that is consumed in the photocatalytic activity, thus reduces the decomposition rate.

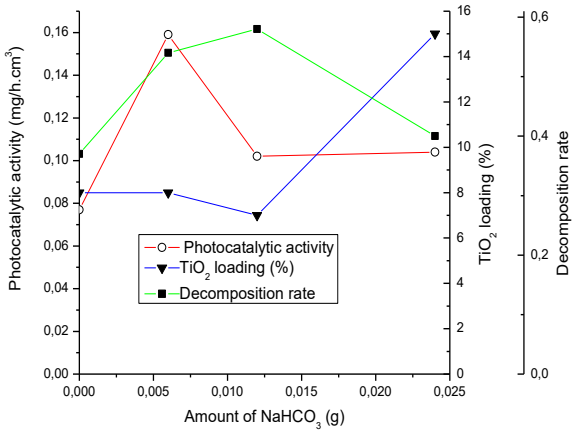

Fig. 5: Effect of the amount of $NaHCO_3$ on photocatalytic properties of poly(PEGDA-co-HEMA)/TiO_2 composite hydrogel.

Effect of PEGDA/HEMA ratio

Results of poly(PEGDA-co-HEMA) hydrogels synthesized at a various PEGDA/HEMA ratio (0.1–10.3 g/g) are given in Fig. 6 (A-H). PEGDA of 4 Kg mol^{-1} molecular weight was used. Although PEGDA/HEMA ratio didn't show remarkable effect on photocatalytic activity, it clearly affected the TiO_2 loading and decomposition rate (Fig. 6A). TiO_2 loadings and decomposition rate of the composite and pore size were found as directly proportional to the PEGDA/HEMA ratio. Before TiO_2 loading, hydrogel (P22) with a higher PEGDA/HEMA ratio showed wide pores (Fig. 6E) in the SEM study. The TiO_2 loadings caused layered pore morphology of the composites (Fig. 6H). Chemical structural similarity between $Ti(OBu)_4$ and PEGDA can causes more $Ti(OBu)_4$ diffusion onto the hydrogel. It means higher PEGDA/HEMA ratio will result more TiO_2 loading.

The increase of decomposition rate with the increasing of PEGDA/HEMA ratio relates to four different factors *i.e.* surface area, crystallinity, chain flexibility and crosslinking density. Surface area of TiO_2 loaded composites increased with PEGDA/HEMA ratio (P22 Fig. 6H). Cross-linked PEGDA molecules have capability to form a crystalline structure and that is directly proportional to the PEGDA/HEMA ratio (DSC results of P22, P24, P25 and P31 in Fig. 6B). Heat flow increased with the increase of PEGDA/HEMA ratio. It means the crystallinity can be increased by increasing the PEGDA/HEMA ratio. High PEGDA/HEMA ratios creates elastic hydrogels despite their increasing crystallinity due to a very low Tg value (-53 ^oC) of PEGDA [30] compared to poly(HEMA) *i.e.* 117 ^oC [36]. PEGDA gives a sharp peak at 63 ^oC [27] in the heat flow, while P22 peak went very near to it *i.e.* at 55 ^oC, after which, the crystallinity does not retain (Fig. 6B). With a decrease in PEGDA/HEMA ratio, the flexible PEGDA/HEMA copolymeric hydrogels turned hard. This was also tested by touching the hydrogels (digital images: left top corners of Fig. 6C, D and E) with the fingers.

Increasing the PEGDA/HEMA ratio caused an increment in crosslinking density and crystallinity, which have a reverse effect on the decomposition rate. However, reducing the hardness of the hydrogel chains by increasing PEGDA/HEMA ratio and surface area showed a positive effect on the decomposition rate. Although there is a competition among the increasing and decreasing decomposition rates factors, increasing factors are more effective. Thus as a whole, increasing the PEGDA/HEMA ratio causes an increase in the decomposition rate.

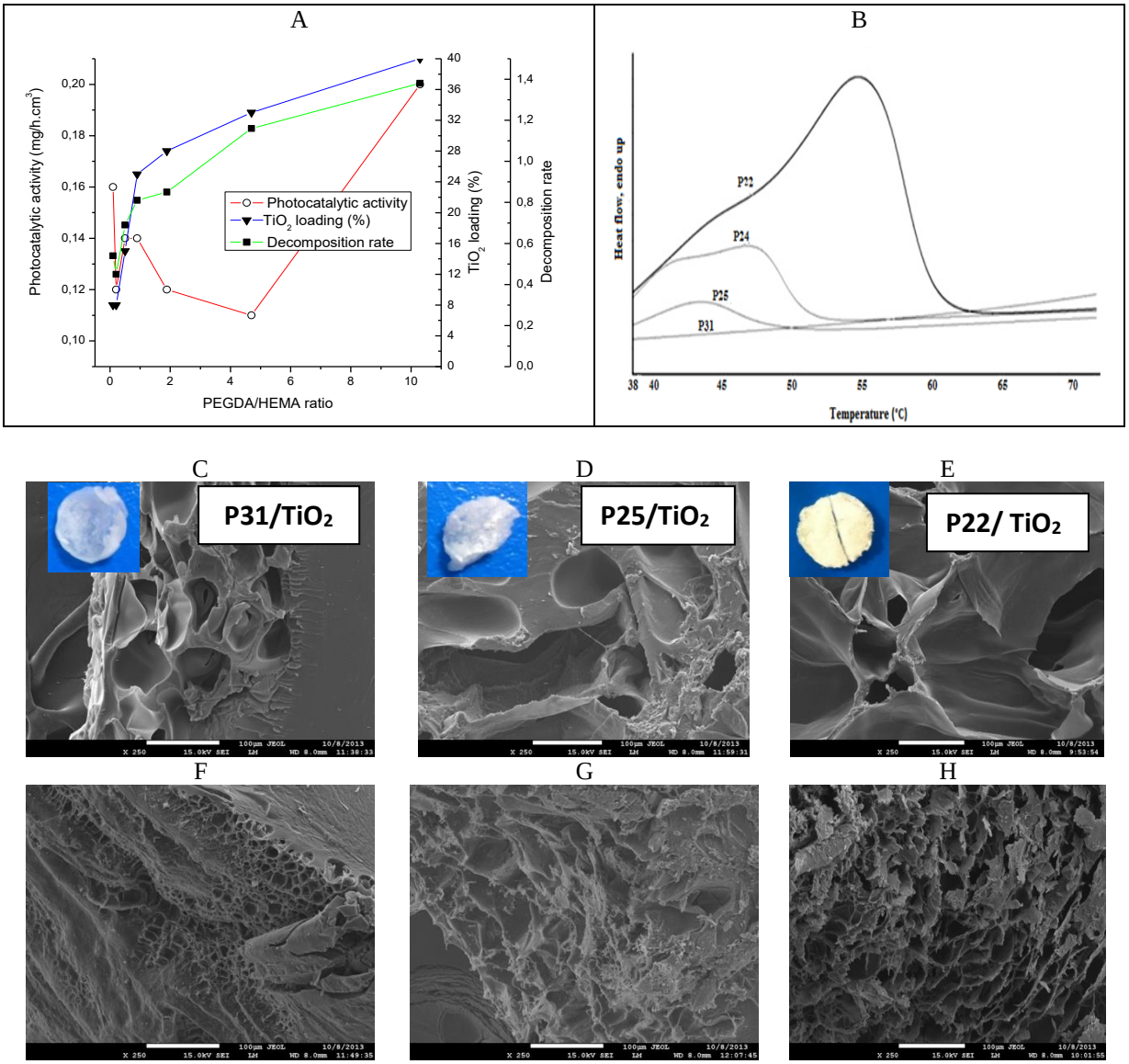

Fig. 6: TEM images showing the effects of PEGDA/HEMA (g/g) ratio on photocatalytic properties of poly (PEGDA-co-HEMA)/TiO_2 composite hydrogels (A), pore morphology of hydrogels: 0.1 (P31) (C), 0.9 (P25) (D), 10.3 (P22) (E) and composite hydrogels: 0.1 (P31) (250x) (F), 0.9 (P25) (G) and 10.3 (P22) (H) and DSC diagrams of hydrogels (B).

Effect of the amount of PEG

Increasing PEG content (0-0.25 g of 4Kg mol^{-1}) did not affect the photocatalytic activity (Fig. 7A) but the pore size of the hydrogels increased (Fig. 7B, C and D). The pore size of the hydrogel decreased after TiO_2 loading (Fig. 7 E). On the other hand, there is no linear relation between TiO_2 loading and PEG content (Fig. 7A); P40 and P38 have similar and wider pores than P39. P38 had a lower TiO_2 content than P40, although it has the highest amount of PEG in the prepared medium. Since P40 hydrogel has homogenous structure (SEM image Fig. 7C) as well as open and regular medium sized pores, it has the highest surface area as well as the highest TiO_2 loading (Fig. 7A). Heterogeneity in P38 (Fig. 7D) duo to the PEGDA and HEMA separately accumulations may have caused ineffective diffusion of $Ti(OBu)_4$ precursor in the hydrogel structure.

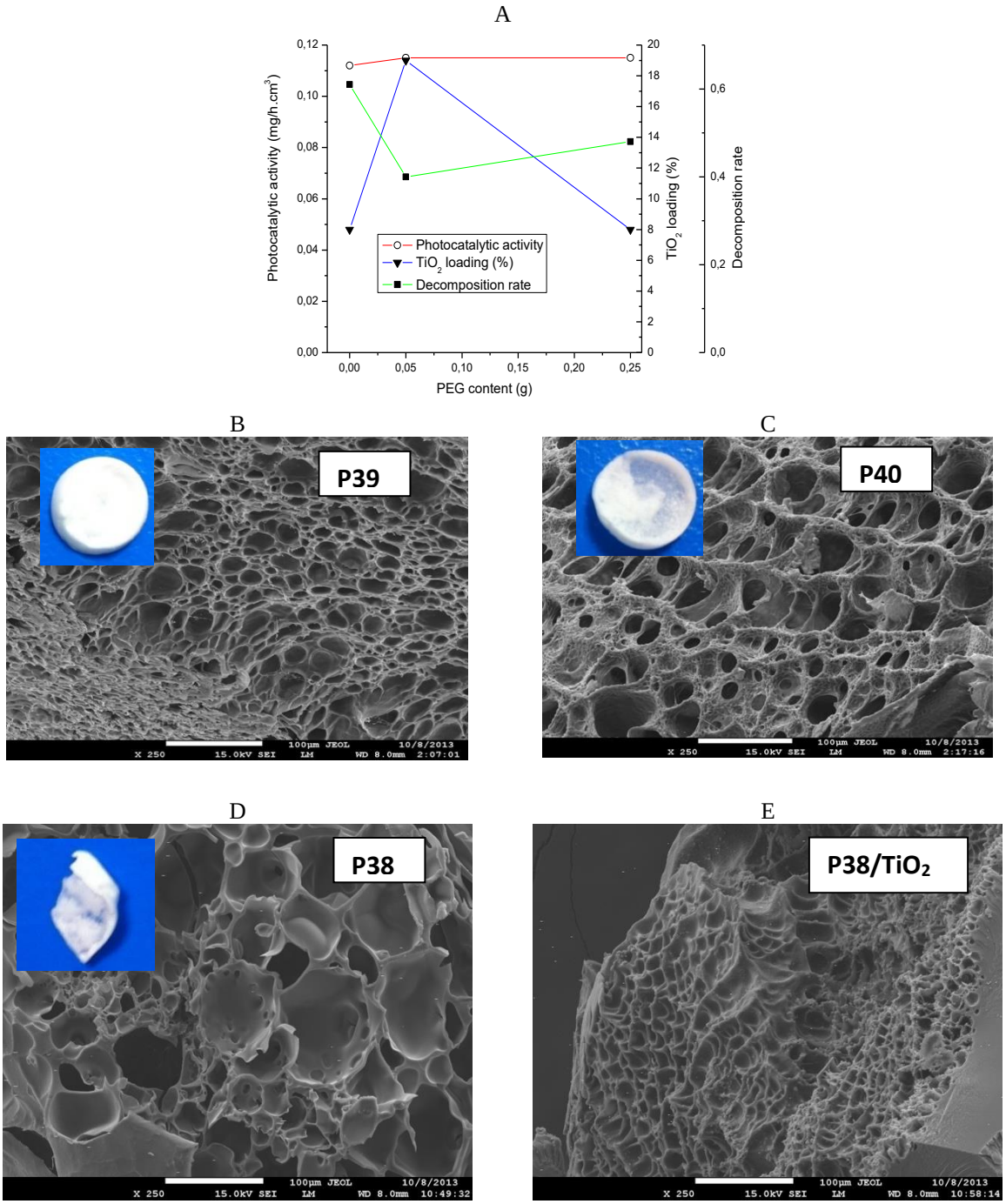

Fig. 7: TEM images showing the effects of PEG content in formulations on photocatalytic activity, TiO2 loading and decomposition rate (A) of P38, P40 and P39 coded hydrogel composites and morphological properties of hydrogels; without PEG (P39) (B), 0,05g (P40) (C), 0,25 g (P38) (D) and composite hydrogel: 0.25 g (P38) (250x)(E).

The decomposition rate decreased with an increase of PEG amount (Fig. 7A). PEG and PEGDA are similar in structures, thus while the synthesis of hydrogel, more amount of PEG would dissolve some of the PEGDA and decrease the PEGDA/HEMA ratio in the hydrogel. As we have seen, the decomposition ratio became higher when PEGDA/HEMA ratio was increased. As the increase of PEG causes decrement in the PEGDA/HEMA ratio, one would expect the downfall in the

decomposition ratio. This assumption was also supported by the touching test of the original lyophilized hydrogels (digital images: top left of Fig. 7 B, C and D). Increasing the PEG content caused the formation of heterogeneous hydrogel formation that contains opaque and transparent sections. In addition, swelling ratio (g water/g dry hydrogel) of P39, P40 and P38 hydrogels were found as 417, 539 and 705, respectively. Higher HEMA content causes an increase in the swelling ratio [32] as reported earlier.

Effect of the monomer concentration

Poly(PEGDA-co-HEMA)/TiO_2 composite hydrogels were prepared using poly(PEGDA-co-HEMA) hydrogels at different concentrations of monomer. In these formulations, PEGDA: HEMA (g/g) ratio was selected to be 2:1. Although increasing the total monomer content caused increments in photocatalytic activity, it caused a decrease in TiO_2 loading (Fig. 8). Increasing the amount of monomer might make the composite hydrogel attractive to the substrate MO. Thus, the photocatalytic rate increased despite decreasing the TiO_2 content. Since increasing the amount of monomer caused the formation of more contact area between polymer and TiO_2 layers, a significant increase in the decomposition rate occurred as was expected.

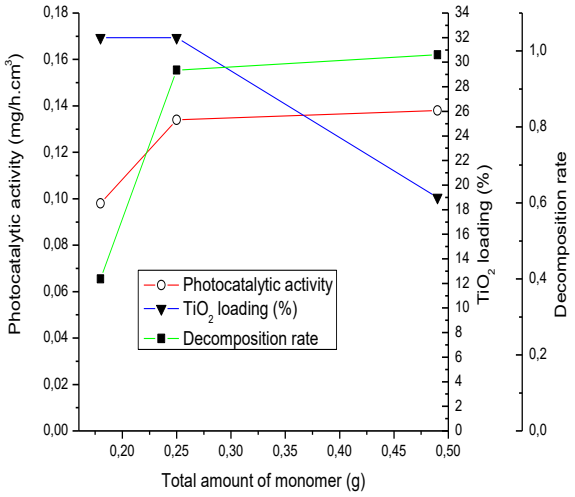

Fig. 8: Effect of amount of total monomer on photocatalytic reduction rate, TiO_2 content and decomposition rate. PEGDA(Mn:4000) / HEMA : 2/1 (g/ml).

Composite hydrogels with slow decomposition rate and long life

The study can lead to two different utilizations: 1) hydrogel composites with slow decomposition rate but longer life, 2) hydrogels composites that leaves TiO_2 skeleton after decomposition of the polymer. This study was mainly aimed to obtain photocatalytic composite hydrogels with slower decomposition rates and higher photocatalytic activity. The study consisted of 28 different formulations and concluded that higher PEGDA/HEMA ratio, lower amounts of PEG and $NaHCO_3$ pore formers and lower molecular weights of PEGDA are suitable characteristics for our desired formulation. Out of the tested samples (Table-1), P41, P42 and P44 were selected for the slow decomposition longer life hydrogel composites. Their TiO_2 content, photocatalytic activity and decomposition rates are presented in Fig. 9.

During the photocatalytic activity, %TiO_2 in composite hydrogel (Fig. 9) was partially increased until 108 hours, but then started to decline. Initially, a little organic part of composite hydrogel and TiO_2 layers decomposed that left behind the TiO_2 and polymeric parts that is stronger than the previous one. The decomposition rate also decreased with the formation of stable TiO_2 layers in the composite structure (Fig. 9). The results obtained in this study are in correspondence with the aim of the study as P41, P42 and P44 hydrogels showed enough photocatalytic activity and low decomposition rate (Fig. 9). Among these, P44, reflected the least decomposition rate, where PEGDA added was of lower molecular weight (400 g mol^{-1}). Smaller PEGDA molecules results higher crosslinking density and less flexibility of high amounts of poly(HEMA) in the composite hydrogel. Generally, poly(HEMA) swells in the presence of water, however, after the TiO_2 loadings, -OH at the terminus are no more available that makes the surface as hydrophobic. Due to that, poly(HEMA) absorbs less water and behaves rigidly. However, the photocatalytic activity of P44 was less than P42. In P44, the average decomposition rate observed was 12 % in 144 hours. Additionally, the TiO_2 amount is also stable. It means both polymeric structure and TiO_2 are uniformly detaching. Due to their tunable degradability as well as hydrophilicity and biocompatibility, poly(PEGDA-co-HEMA)/TiO_2 composites can be used in artificial skin [16] and skin care [37].

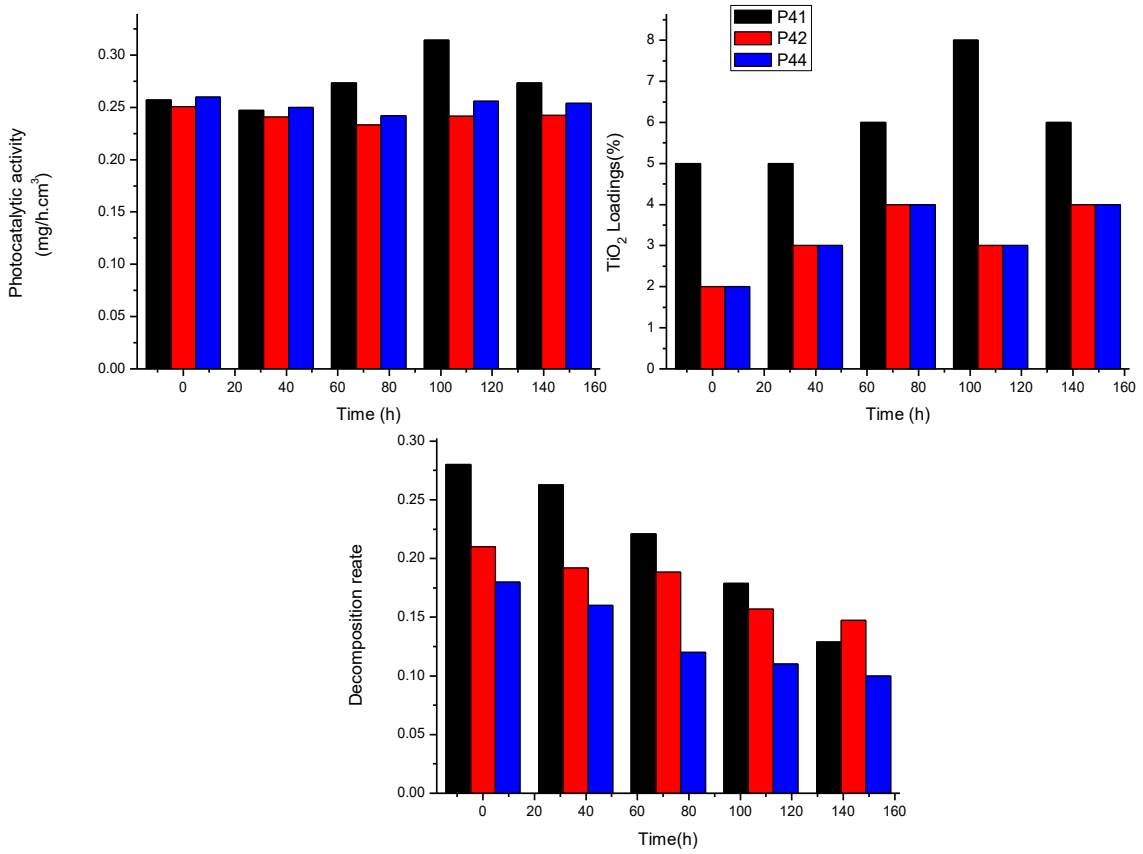

Fig. 9: Determination of photocatalytic properties of P41, P42 and P44 composite hydrogels with duration of photocatalytic activity.

Composite hydrogels that leaves TiO_2 skeleton after decomposition

Utilizing the tunability of the composite hydrogels, polymeric structures were prepared with higher TiO_2 amounts. This type of hydrogels can be used for long term decomposition of the contaminant substrates, but the polymer also decomposes in the meanwhile by the TiO_2. The degraded polymeric parts can be washed out to left behind a TiO_2 template that will have a higher surface area and pores. This type of TiO_2 entities were observed in the formulations where PEGDA/HEMA ratio was higher e.g. P9 (SEM image Fig. 10 C). To verify this assumption, % of TiO_2 content relative to its initial value in the composite hydrogel, % decomposition, % of TiO_2 in the composite matrix and photocatalytic activity were plotted versus photocatalytic activity time (Fig. 10). The Fig. 10A has three parts; the loaded % of TiO_2, decomposition of the polymer and the TiO% in the composite. Initially, the loaded TiO_2 is 100% whereas in the composite, it is 30 % only. As the photocatalytic activity goes on, the % loaded TiO_2 decreased for a while, then get constant. On the other hand, decomposition of the polymer occurred that increased the % TiO_2 in the composite (108 h). These lines can safely conclude that after 100 % decomposition, the composite will be 100 % TiO_2 skeleton. The SEM images of P9 before (Fig. 10C) and after TiO_2 loading at 36 (Fig. 10D), 72 (Fig. 10E) and 108 (Fig. 10F) hours also support these results. The SEM images clearly reflect that as the decomposition goes on, % TiO_2 layer and pore sizes increased. After 108 h of the photocatalytic activity of MO, most of the polymer from the surface is replaced by the TiO_2 layer (Fig. 10F). The amount of TiO_2 after 108 hours on the surface in more as compared to the surface after 72 hours as seen from the SEM images.

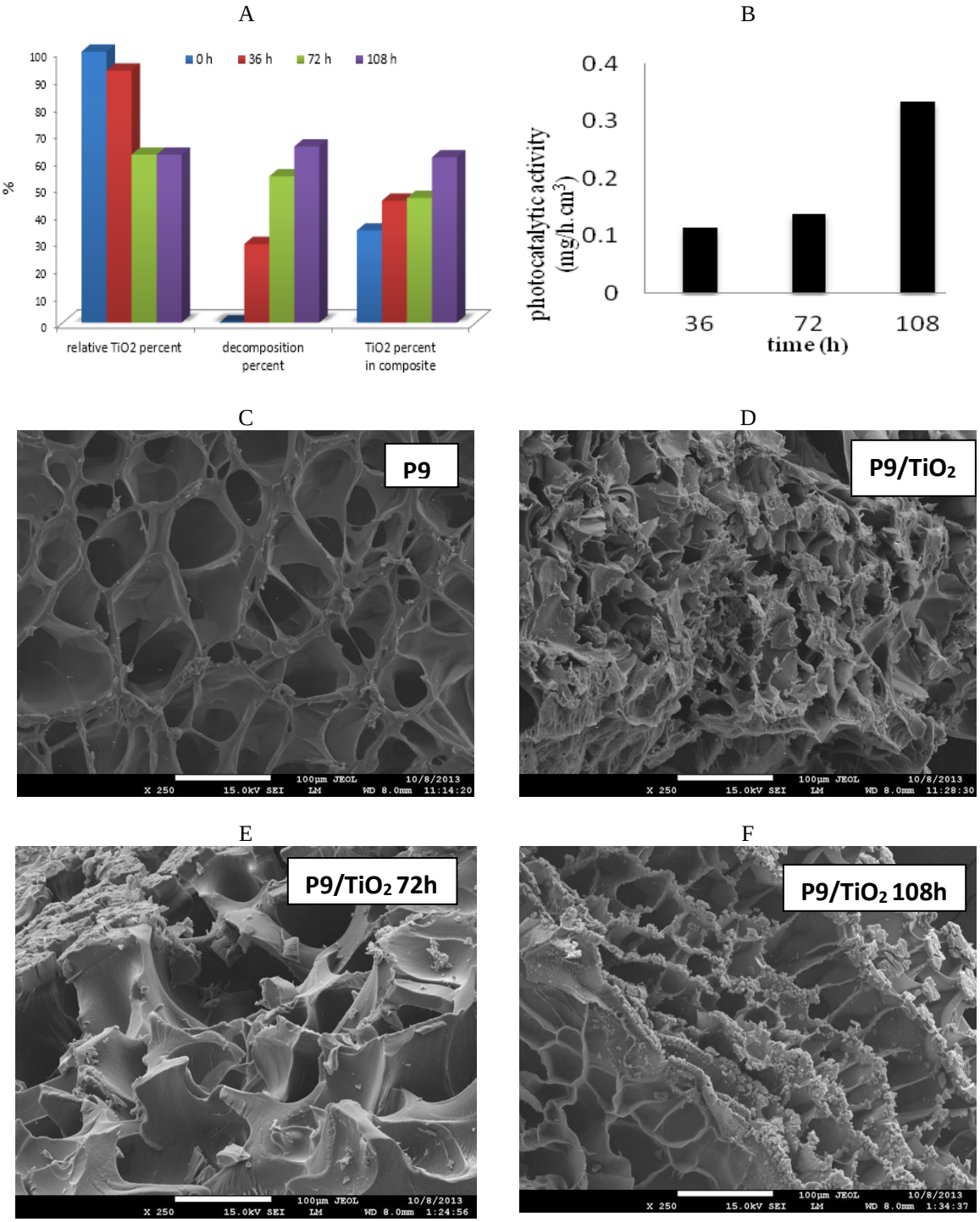

Fig. 10: TEM images showing the decomposition behavior of P9 coded poly(PEGDA-co-HEMA)/TiO_2 composite hydrogel with photocatalytic activity time: on the base of TiO_2 content (A) and photocatalytic activity (B) and pore morphology with SEM photographs (C, D, E and F).

The above discussion reveals that the highest photocatalytic activity of poly(PEGDA-co-HEMA)/TiO_2 composite hydrogels is approximately 1 mg MO/(g composite hydrogel x hour). Few studies that used polymeric carriers are summarized in Table-2. Generally methylene blue (MB) is used as substrate in studies with higher photocatalytic rates [900 mg MB/(g nanofiber hour)] [16]. The

microsphere form of carriers showed less catalytic performance relative to nanofibers, as expected [10,12]. We have tried MB but it was not stable and decomposed quickly; with or without sunlight. However, MO was very stable, and its decomposition rate was very slow under sunlight. Thus, we chose MO for catalytic activity. As the MB decomposition rate is very high with nanofibers, it is not suitable to compare with the results obtained with MO with our composite hydrogels. Additionally, there is no photocatalytic activity in the literature performed by the hydrogels.

We can compared our results with TiO_2 encapsulated poly(DVB) microspheres (PDVB@TiO_2) of 2-3 µm diameter [10] and monodisperse poly (EGDMA-co-MAA))/SiO_2/ Poly (EGDMA-co-MAA)/TiO_2 microspheres of 0.5 µm [12] that provided photocatalytic reduction performance at 10 mg MB/ (g composite particle x hour) and 50 mg MO/(g hollow microsphere x hour), respectively. Although their large surface area calculated (considering their external surface) was approximately 1,000–10,000 times higher than our composite hydrogels, our composite hydrogels presented only 10–50 times less photocatalytic activity than these microspheres. The performance of our hydrogels are also comparable with TiO_2 nanofibers [38] with 5 mg Rhodamine B (RHB)/(g TiO_2 nanofiber hour) photocatalytic activity. These results clearly demonstrate the significance and effectiveness of poly(PEGDA-co-HEMA)/TiO_2 composites that can be prepared in macro-sizes.

Conclusion

This study was mainly aimed to obtain easily producible photocatalytically active TiO_2 carrying composites. For this purpose, the porous hydrogels with different morphologies were used in TiO_2 loading using an acid peptization method at room temperature. This is the first report of hydrogel composites at such moderate temperature. TiO_2 loading and decomposition of TiO_2/Poly(PEGDA-co-HEMA) composite hydrogels can be tuned by changing hydrogel composition and pore morphology. Although some formulations (out of 28) presented very slow decomposition rate of methyl orange, others were rapid, but they left behind porous TiO_2 skeleton that are suitable for long-term and high-speed photocatalytic applications. The composites with these properties can be used in the in skin-tissue engineering. Additionally, these composites can be used to decompose organics from wastewaters, sea as well as pools. These hydrogel composites are very versatile, tunable and can be used in various fields e.g. antifungal applications on skins etc.

Table-2: Comparison of photocatalytic activity of Poly(PEGDA-co-HEMA)/TiO_2 composite hydrogels to the literature.

Composite Polymer	Preparation method	Substrate	Radiation System	Photocatalytic Rate (mg substrate/g composite · hour)	Reference
Poly(MAA-co-TFA)/PVDF nanofiber mat	Electrospinned fiber + titanium oxosulphate + H_2SO_4 + urea + 150°C autoclaved	MB	15W, 254 nm UV lamps	900 mg MB/g nanofiber	[18]
(Poly(EGDMA-co-MAA))/ SiO_2/Poly(EGDMA-co-MAA)/TiO_2 (approximately 0.5 micron size)	550°C, calcination for 4 hours	MO	500 W high pressure mercury lamp	50 mg MO/g hollow microsphere	[12]
TiO_2 encapsulated poly(DVB) microspheres (PDVB@TiO_2) in 2–3 micron size	λ-[(methacryloxy) propyl] trimethoxy silane + DVB + AIBN + $(Ti(OBu)_4$ + 10% HCl, and hydrolyzing + acid peptization at 80°C for 8 hours	MB	300 W Osram lamp, λ = 365 nm	10 mg MB/g composite particle	[10]
TiO_2 nanofiber	Tetrabutyl titanate + PVP + electrospinning + calcination at 700°C for 3 hours	RHB	500W tungsten halogen lamp λ >420 nm	5 mg Rhodamine B (RHB)/g TiO_2 nanofiber	[38]
Poly(PEGDA-co-HEMA) composite copolymer	Poly(PEGDA-co-HEMA) hydrogel+ $Ti(OBu)_4$ +HNO_3 peptization, room conditions	MO	300 W Osram lamps mainly λ λ = 365 nm, (simulate sun light)	1 mg MO/ g composite hydrogel	This study

Acknowledgements

We are grateful to the Scientific Research Projects Office of Mugla Sitki Kocman University (Project number BAP-12/109) for their financial support. The authors wish to thank Prof. Dr. Ahmet Balci for his equipment support

References

1. T. Heberer, and T. Heberer, Occurrence, fate, and removal of pharmaceutical residues in the aquatic environment: a review of recent research data., *Toxicol. Lett.*, **131**, 5 (2002).
2. K. Kümmerer, A. Al-Ahmad, and V. Mersch-Sundermann, Biodegradability of some antibiotics, elimination of the genotoxicity and affection of wastewater bacteria in a simple test, *Chemosphere*., **40**, 701 (2000).
3. T. A. Ternes, Occurrence of drugs in German sewage treatment plants and rivers, *Water Res.*, **32**, 3245 (1998).
4. H. Zhang, X. Quan, S. Chen, H. Zhao, and Y. Zhao, Fabrication of photocatalytic membrane and evaluation its efficiency in removal of organic pollutants from water, *Sep. Purif. Technol.*, **50**, 147 (2006).
5. M. R. Hoffmann, S. Martin, W. Choi, and D. W. Bahnemannt, Environmental Applications of Semiconductor Photocatalysis, *Chem. Rev.*, **95**, 69 (1995).
6. L. Zhang, T. Kanki, N. Sano, and A. Toyoda, Development of TiO2 photocatalyst reaction for water purification, *Sep. Purif. Technol.*, **31**, 105 (2003).
7. J. Augustynski, The role of the surface intermediates in the photoelectrochemical behaviour of anatase and rutile TiO2, *Electrochim. Acta*., **38**, 43 (1993).
8. L. Znaidi, R. Séraphimova, J. F. Bocquet, C. Colbeau-Justin, and C. Pommier, A semi-continuous process for the synthesis of nanosize TiO2 powders and their use as photocatalysts, *Mater. Res. Bull.*, **36**, 811 (2001).
9. F. Mazille, T. Schoettl, N. Klamerth, S. Malato, and C. Pulgarin, Field solar degradation of pesticides and emerging water contaminants mediated by polymer films containing titanium and iron oxide with synergistic heterogeneous photocatalytic activity at neutral pH, *Water Res.*, **44**, 3029 (2010).
10. Z. Liuxue, L. Peng, and S. Zhixing, A low temperature preparation and photocatalytical activities of PDVB@TiO2 hybrid microspheres, *J. Mater. Sci.*, **41**, 7218 (2006).
11. L. H. Lin, H. J. Liu, J. J. Hwang, K. M. Chen, and J. C. Chao, Photocatalytic effects and surface morphologies of modified silicone-TiO2 polymer composites, *Mater. Chem. Phys.*, **127**, 248 (2011).
12. H. Zhang, X. Zhang, and X. Yang, Facile synthesis of monodisperse polymer/SiO2/polymer/TiO2 tetra-layer microspheres and the corresponding double-walled hollow SiO2/TiO2 microspheres, *J. Colloid Interface Sci.*, **348**, 431 (2010).
13. C. A. Coutinho, and V. K. Gupta, Photocatalytic degradation of methyl orange using polymer-titania microcomposites, *J. Colloid Interface Sci.*, **333**, 457 (2009).
14. W. Kangwansupamonkon, W. Jitbunpot, and S. Kiatkamjornwong, Photocatalytic efficiency of TiO2/poly[acrylamide-co-(acrylic acid)] composite for textile dye degradation, *Polym. Degrad. Stab.*, **95**, 1894 (2010).
15. V. K. Konaganti, and G. Madras, Photooxidative and pyrolytic degradation of methyl methacrylate-alkyl acrylate copolymers, *Polym. Degrad. Stab.*, **94**, 1325 (2009).
16. Y. Haldorai, and J.-J. Shim, Novel chitosan-TiO_2 nanohybrid: Preparation, characterization, antibacterial, and photocatalytic properties, *Polym. Compos.*, **35**, 327 (2014).
17. P. A. Tran, D. P. Biswas, and A. J. O'Connor, Simple one-step method to produce titanium dioxide-polycaprolactone composite films with increased hydrophilicity, enhanced cellular interaction and improved degradation for skin tissue engineering, *J. Mater. Sci.*, **49**, 6373 (2014).
18. T. He, Z. Zhou, W. Xu, F. Ren, H. Ma, and J. Wang, Preparation and photocatalysis of TiO2-fluoropolymer electrospun fiber nanocomposites, *Polymer (Guildf).*, **50**, 3031 (2009).
19. S. Padhi, P. G. R. Achary, and N. C. Nayak, Mechanical and morphological properties of halloysite nanotubes filled ethylene-vinyl acetate copolymer nanocomposites, *Indian J. Chem. Technol.*, **24**, 184 (2017).
20. Q. Yin, J. Xiang, X. Wang, K. Zhang, X. Guo, and G. Shen, Synthesis of highly crystalline mesoporous TiO2 by a fast sol-gel method, *Indian J. Chem. Technol.*, **24**, 223 (2017).
21. B. Sarkar, S. Suman, R. Tiwari, R. K. Singha, S. Ghosh, S. Acharyya, and R. Bal, Pt nanoparticles supported on mesoporous ZSM-5: A potential catalyst for reforming of methane with carbon dioxide, *Indian J. Chem. Technol.*, **51**, 1348 (2012).
22. S. Yamazaki, N. Fujinaga, and K. Araki, Effect of sulfate ions for sol-gel synthesis of titania photocatalyst, *Appl. Catal. A Gen.*, **210**, 97

(2001).
23. T. Zeng, Y. Qiu, L. Chen, and X. Song, Microstructure and phase evolution of TiO2 precursors prepared by peptization-hydrolysis method using polycarboxylic acid as peptizing agent, *Mater. Chem. Phys.*, **56**, 163 (1998).
24. B. L. Bischoff, and M. A. Anderson, Peptization Process in the Sol-Gel Preparation of Porous Anatase (TiO2), *Chem. Mater.*, **7**, 1772 (1995).
25. J. Wang, X. Han, C. Liu, W. Zhang, R. Cai, and Z. Liu, Adjusting the Crystal Phase and Morphology of Titania via a Soft Chemical Process, *Cryst. Growth Des.*, **10**, 2185 (2010).
26. S. J. Im, Y. M. Choi, E. Subramanyam, K. M. Huh, and K. Park, Synthesis and characterization of biodegradable elastic hydrogels based on poly(ethylene glycol) and poly($ε$-caprolactone) blocks, *Macromol. Res.*, **15**, 363 (2007).
27. S. Kaewpirom, and S. Boonsang, Electrical response characterisation of poly(ethylene glycol) macromer (PEGM)/chitosan hydrogels in NaCl solution, *Eur. Polym. J.*, **42**, 1609 (2006).
28. A. J. Mcevoy, and M. Gr, Influence of precursors on the morphology and performance of Ti02 photoanodes, **26**, 3305 (1991).
29. J. Yang, S. Mei, and M. F. Ferreira, Hydrothermal Synthesis of Nanosized Titania Powders : Influence of Peptization and Peptizing Agents on the Crystalline Phases and Phase Transitions, *Synthesis (Stuttg).*, **68**, 1361 (2000).
30. Y. M. Lee, S. S. Kim, and S. H. Kim, Synthesis and properties of poly(ethylene glycol) macromer/beta-chitosan hydrogels., *J. Mater. Sci. Mater. Med.*, **8**, 537 (1997).
31. A. G. P. R. Figueiredo, A. R. P. Figueiredo, A. Alonso-varona, S. C. M. Fernandes, T. Palomares, E. Rubio-azpeitia, A. Barros-timmons, A. J. D. Silvestre, C. P. Neto, and C. S. R. Freire, Biocompatible bacterial cellulose-poly(2-hydroxyethylethacrylate) Nanocomposite Films, *Biomed Res Int.*, 698141 (2013).
32. G. Tan, Y. Wang, J. Li, and S. Zhang, Synthesis and characterization of injectable photocrosslinking poly (ethylene glycol) diacrylate based hydrogels, *Polym. Bull.*, **61**, 91 (2008).
33. K. Thamaphat, P. Limsuwan, and B. Ngotawornchai, Phase Characterization of TiO2 Powder by XRD and TEM, *Nat. Sci.*, **42**, 357 (2008).
34. A. Salerno, S. Zeppetelli, E. Di Maio, S. Iannace, and P. A. Netti, Architecture and properties of bi-modal porous scaffolds for bone regeneration prepared via supercritical {CO2} foaming and porogen leaching combined process, *J. Supercrit. Fluids*., **67**, 114 (2012).
35. R. Seda Tiğli, A. Karakeçili, and M. Gumusderelioglu, In vitro characterization of chitosan scaffolds: Influence of composition and deacetylation degree, *J. Mater. Sci. Mater. Med.*, **18**, 1665 (2007).
36. D. S. Jones, C. P. Lorimer, C. P. McCoy, and S. P. Gorman, Characterization of the physicochemical, antimicrobial, and drug release properties of thermoresponsive hydrogel copolymers designed for medical device applications, *J. Biomed. Mater. Res. - Part B Appl. Biomater.*, **85**, 417 (2008).
37. Q. Huang, Z. Jiao, M. Li, D. Qiu, K. Liu, and H. Shi, Preparation, characterization, antifungal activity, and mechanism of chitosan/TiO 2 hybrid film against bipolaris maydis, *J. Appl. Polym. Sci.*, **128**, 2623 (2013).
38. J. Li, H. Qiao, Y. Du, C. Chen, X. Li, J. Cui, D. Kumar, and Q. Wei, Electrospinning Synthesis and Photocatalytic Activity of Mesoporous TiO2 Nanofibers, *Sci. World J.* 1 (2012).